JOURNAL OF MATERIALS SCIENCE 33 (1998) 4111–4119

Sol–gel processing of hydroxyapatite

A. JILLAVENKATESA, R. A. CONDRATE SR
New York State College of Ceramics, Alfred University, Alfred, NY 14802, USA
E-mail: fcondrate@bigvax.alfred.edu

Hydroxyapatite, a calcium phosphate-based compound with numerous applications in the biological field was synthesized using the sol–gel processing route. The formation of hydroxyapatite and other compounds during the heat-treatment cycle were identified and characterized using thermal analyses and X-ray diffraction together with infrared and Raman spectroscopy. The influence of the addition of various organic alcohols (R–OH, R=CH_3–, C_2H_5– and C_3H_8–) on the reaction results was studied. © *1998 Kluwer Academic Publishers*

1. Introduction

Hydroxyapatites ($Ca_{10}(PO_4)_6(OH)_2$) are a class of calcium phosphate-based materials that have been of immense interest for biomedical applications [1, 2]. The widespread use of hydroxyapatite in these applications arises due to the chemical similarity between hydroxyapatite and the mineral part (calcified tissue) of human bone. Hydroxyapatite constitutes approximately 70% (by weight) of natural bone [2], The term "apatite" applies to a broad category of structures comprised of different constituents. Hydroxyapatite is one such constituent, another being carbonate (hydroxy)apatite, where carbonate ions may substitute for some of the hydroxyl ions (A-type) or the carbonate ions may be present on the phosphate sites (B-type) [3, 4]. In addition to hydroxyapatite, a small amount of B-type carbonate apatite is also present in the human body. This apatite is also known as biological apatite and contains small amounts of sodium, potassium, magnesium fluoride and chloride ions [5]. Given the numerous applications of hydroxyapatite in biomedical fields, numerous techniques for synthesis of hydroxyapatite have been developed.

One of the earliest techniques developed for the synthesis of hydroxyapatite involved the hydrothermal conversion of fluorapatite ($Ca_{10}(PO_4)_6F_2$) to hydroxyapatite under a pressure of 5000 p.s.i. (10^3 p.s.i. = 6.87 N mm^{-3}) and temperature range of 920–1230 °C [6]. Hydrothermal preparation of hydroxyapatite has also been performed using various calcium and phosphate precursors including (a) anhydrous dicalcium phosphate ($CaHPO_4$), phosphoric acid and dicalcium phosphate dihydrate ($CaHPO_4 \cdot 2H_2O$) [7], and (b) calcium acetate and triethyl phosphate ($PO(OC_2H_5)_3$) [8]. In this type of preparation, the formation of hydroxyapatite as the final product may be preceded by the formation of intermediate products such as β-calcium pyrophosphate ($Ca_2P_2O_7$) or calcium monohydrogen phosphate ($CaHPO_4$) depending upon the applied temperature and pressure.

The most commonly used technique for the formation of hydroxyapatite is the precipitation technique involving wet chemical reactions between the calcium and phosphate precursors under controlled temperature and pH conditions. A commonly used aqueous precipitation technique involves a reaction between stoichiometric amounts of ammonium phosphate ($(NH_4)_2HPO_4$) and calcium nitrate under a pH of 10, and at 60 °C. After suitable ageing and drying, the precipitate is calcined at temperatures of 400–600 °C followed by sintering between 1000 and 1200 °C [9, 10]. A major concern here is to maintain the pH level greater than 9, as a reduction in the pH leads to the formation of calcium-deficient apatite structures. Furthermore, the formation of hydroxyapatite is not complete until the final stages of sintering, and often sintering at elevated temperatures leads to the decomposition of hydroxyapatite leading to the formation of tricalcium phosphate. The conventional sintering step has been eliminated in the technique developed by Lerner *et al.* [11] who utilized microwave irradiation to enhance the seed crystals of hydroxyapatite. The presence of any foreign impurities in the chemical precursors may lead to their incorporation into the formed apatitic structures. Low-temperature formation of stoichiometric hydroxyapatite by diffusional-control mechanisms involving solid-state reactants (dicalcium phosphate, $CaHPO_4$, and tetracalcium phosphate, $Ca_4(PO_4)_2O$), in an acid–base reaction has been reported by Brown *et al.* [12, 13].

Other techniques of hydroxyapatite formation have involved the hydrolysis of a suitable calcium phosphate precursor (dicalcium phosphate dihydrate ($CaHPO_4 \cdot 2H_2O$)) [14], calcination of freeze-dried mixtures [15], and the incorporation of calcium and phosphate ions in an agar-gel system to form calcium-deficient hydroxyapatite fibres [16]. Hu *et al.* [17] have reported the formation of hydroxyapatite from phosphate-rich glasses formed by the reaction of calcium nitrate and phosphoric acid with the aid of accoustic waves to enable the maturation of the grains.

The sol–gel processing technique which affords greater control over the formation of particular phases and the purity of the formed phases, and lower processing temperatures has, however, not been applied extensively to the formation of hydroxyapatite powders, films or bulk forms. The major limitations in its application have been due to the drawbacks associated with hydrolysis of phosphates [18], and the higher cost of raw materials, when compared to the cost of chemicals used in conventional techniques such as precipitation or hydrothermal techniques. Phosphate esters, being very stable towards water, cannot be hydrolysed easily and the hydrolysis may be possible only in the presence of metal-ion containing catalysts. Phosphoric acid, however, has an extremely rapid reaction rate leading to precipitation of phosphate rather than hydrolysis. Deptula *et al.* [19] developed a water extraction variant of the sol–gel process in which hydroxyapatite spheres were formed by a repetitive process of emulsification of a mixture of calcium acetate and phosphoric acid followed by the solidification of this emulsion by the extraction of water. The spheres were then calcined to form hydroxyapatite. Thin films of hydroxyapatite using the sol–gel route have been developed by Chai *et al.* [20] who used sol–gel solutions made of calcium diethoxide or calcium propionate with triethyl phosphite in ethanol. These films were dip-coated on to various substrates.

The aim of the present work was to synthesize hydroxyapatite powders using a sol–gel route with simple procedures and relatively inexpensive chemicals. This would enable an understanding of the means available to overcome the limitations of the extremely slow rate of hydrolysis of phosphate esters. The influence of slight variations in the stoichiometry of the precursors on the final formed phase was also studied. The role of different alcohols added with the calcium and phosphate precursors was examined.

2. Experimental procedure

2.1. Sol–gel synthesis

The precursors used in this study of sol–gel processing of hydroxyapatite were calcium acetate^{+} ($Ca(C_2H_3O_2)_2$ Sigma Chemicals, St Louis, MO) as the source of calcium ions, and triethyl phosphate ($PO(OC_2H_5)_3$ Fluka Chemicals, Ronkonkoma, NY) as the phosphate precursor. Four batches of sols were made with the calcium and phosphate precursors, and different alcohol (R–OH) types. 0.02 mol calcium acetate was weighed into a nalgene beaker, to which a 0.012 mol triethyl phosphate was added dropwise to attain a Ca/P molar ratio of 1.67. No alcohol was added to one sol batch, while 5 ml methanol (CH_3OH), 5 ml ethanol (C_2H_5OH) or 5 ml propanol ($CH_3CHOHCH_3$) were added to the remaining batches. All of the sample batches were prepared in a controlled environment chamber with flowing nitrogen. The beakers were covered and placed on a magnetic stirrer, and the sols were stirred vigorously for 12 h at 25–30 °C. The temperature was raised to 40–45 °C and maintained for 12 h, while continuously stirring. The batches were then held at 75 °C for 10 h, during which time progress of gelation in the sols was observed. The formed gels were then dried at 120 °C for 10 h.

The dried gels were heat treated at 1000 °C, and the resultant solid was crushed into a fine powder. The powders were examined by X-ray diffraction techniques to determine the phases formed. The powders were then dispersed in a 0.01 M HCl solution and stirred for 2 h. After stirring, the solution was filtered through a Whatman no. 42 filter paper, and the residue on the filter paper was dried at 120 °C for 2 h. The dried powders were then characterized using X-ray diffraction along with Fourier Transform–Infrared (FT–IR) and Raman spectroscopy. Thermal analysis including differential thermal analysis and thermogravimetric analysis were used to detect changes occurring during the heat-treatment process. A flow chart depicting the various steps involved in this process is illustrated in Fig. 1.

2.2. X-ray diffraction characterization

All X-ray diffraction (XRD) patterns were obtained using a Kristalloflex 810 X-ray diffractometer (Siemens, Munich, Germany). Samples for XRD characterization were prepared by mounting finely crushed grains on a zero-background holder. The sample was irradiated with CuK_{α} radiation having a wavelength of 0.154 12 nm, and was generated under an accelerating potential of 40 kV and a beam current of 30 mA. The diffraction patterns were studied using the *EVA/DIFFRAC-AT* software package (EVA: SOCABIM, Paris, France).

2.3. FT–IR and Raman spectral characterization

A Nicolet 60 SX mid-IR spectrometer (Nicolet Instrumets Corporation, Madison, WI) was used for obtaining the mid-IR FT–IR spectra of the samples. All samples were examined in the transmission mode. Samples were mounted in the form of KBr pellets made by thoroughly mixing 1 mg sample powder with 300 mg KBr and pressing in a vacuum die at 1200 p.s.i. (10^3 p.s.i. = 6.89 N mm^{-2}) The instrument possessed a spectral resolution of 4 cm^{-1}.

Raman spectral characterization of the samples were performed using a Spex Industries ISA U-1000 Mole double monochromator Raman Spectrometer (ISA Spex Industries, NJ). An excitation radiation of 514.532 nm wavelength with a laser power of 100 mW at the sample was generated from a Coherent Innova 90 Al^{+} ion laser source (Coherent lasers, Palo Alto, CA). The powdered samples were enclosed within a 1 mm thin-walled glass capillary tube, and the sample was studied under a 180° scattering geometry. The instrument was externally calibrated using the 142 cm^{-1} band observed for the Anatase phase of TiO_2. The spectral resolution of the instrument was approximately 4.0 cm^{-1}.

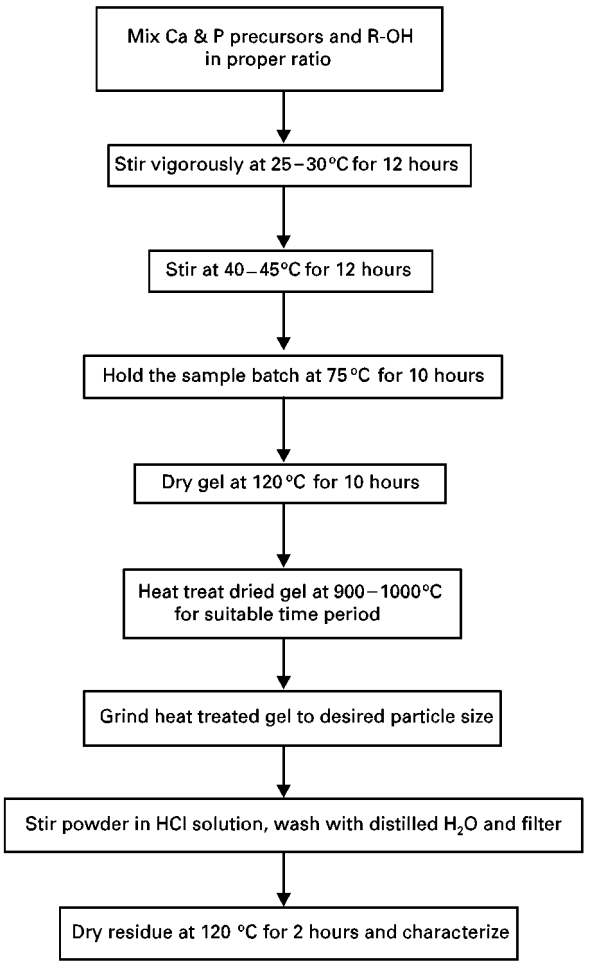

Figure 1 Flow chart indicating the steps involved in synthesis of hydroxyapatite by a sol–gel route.

3. Results and discussion

3.1. Sol–gel process for synthesis of hydroxyapatite

Upon initial mixing of calcium acetate, triethyl phosphate and the appropriate alcohol, the pH of the batch was observed to vary as a function of the added alcohol. The sol–gel batch containing no alcohol was initially observed to be very basic with a pH of 11.25. The pH of the batches containing alcohol was influenced by the alcohol type with the batch containing methanol having a pH of 8.47, the batch with ethanol having a pH of 9.27, and the batch with propanol having a pH of 10.01. No significant changes were observed in the batches while stirring at 25–30 °C for 12 h. Upon continuation of stirring after increasing the temperature to 40 °C, changes in viscosity were observed towards the end of this stirring period. The batch devoid of alcohol showed an increase in viscosity, but was still fluid. The batches containing methanol and ethanol also showed some increase in viscosity, but this increase was less than that observed for the batch containing just the calcium and phosphate precursors. No comparable changes were observed in the viscosity of the batch containing propanol. While holding the batches at 75 °C, significant changes were observed in the gelation times for the various batches. The batch with added propanol increased significantly in viscosity, but had not gelled completely at the end of this treatment period. The sol–gel batch lacking any alcohol formed a highly viscous gel within an hour of being heated at 75 °C. The batches containing methanol and ethanol took longer times to form gel structures, but gelation was complete during the 10 h holding period at 75 °C. Correspondingly, upon drying at 120 °C, the batch containing no alcohol formed a very hard dried gel. The batches containing methanol and ethanol also formed a dry gel. An incompletely dried gel was observed in the case of the batch containing propanol, as was evident from the slightly plastic nature of the gel formed. This batch had to be dried at 120 °C for an additional 8 h.

Differences in the initial pH of the sol–gel batches can be attributed to the nature of the alcohol groups added to the sol–gel batches. Short-chain carbon compounds reduce the pH of the sol to a greater extent than long-chain carbon compounds. The size of the carbon chain has a definite role in the gelation characteristics. The shortest gelation time was observed for the sol–gel batch with no alcohol, while the longest gelation time was observed for the batch mixed with an alcohol containing longer carbon chains. This can be explained by the fact that the gels formed in this case are colloidal gels rather than polymeric gels. This is based on the fact that the hydrolysis rates of phosphate esters ($PO(OR)_3$, R = methyl, ethyl, butyl groups) are exceedingly slow [21], and importantly, no external hydrolysing agent was added to enable the nucleophilic addition of a negatively charged group ($HO^{\delta-}$) to the positively charged metal atom $P^{\delta+}$ which would increase the coordination number of the metal atom (the first step towards a polymerization reaction). Additional evidence of the colloidal nature of the gel lies in the fact that the gelation process is an irreversible process, with the gel not dissolving upon cooling of the gel during the early stages of gelation. The increase in gelation times with increasing carbon atoms in the chain can be explained by the lower volatility of the higher carbon alcohols as compared to the higher volatility of the lower carbon alcohols.

3.2. Thermal analyses of dried gels

The dried gel batches were studied using thermal analyses techniques of differential thermal analysis (DTA) and thermogravimetric analysis (TGA). The DTA traces of the four sol–gel batches with an initial Ca/P molar ratio of 1.67 are illustrated in Fig. 2. Fig. 3 illustrates the changes measured by DTA and TGA, occurring in the dried gel powder containing 5 ml ethanol upon heating to 1000 °C at the rate of 10 °C min^{-1}. From Fig. 2, we observe no significant differences in the DTA trace of the four sol–gel batches. Slight differences are observed in the temperatures at which significant exothermic and endothermic reactions occur at elevated temperatures. The strong endotherms were observed to lie between approximately 500 and 515 °C for the four sample batches. Similarly, strong exotherms were observed between 865 and 880 °C for the four batches. From the

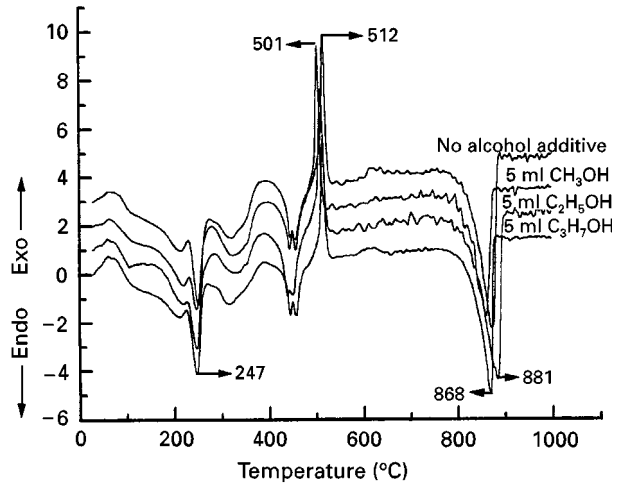

Figure 2 DTA plots for sample batches with different R–OH additives, but all with Ca/P = 1.67.

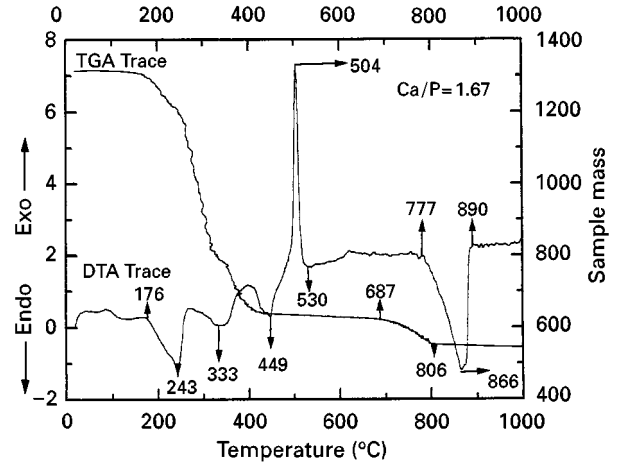

Figure 3 DTA and TGA trace for a sample batch with 5 ml ethanol.

DTA and TGA plots in Fig. 3, slight perturbations are observed in the baseline at very low temperatures. These perturbations can be attributed to the instrument signal stabilization and the evolution of any moisture present in the system. A steady loss in sample mass is observed from about 160 °C up to about 445 °C. From the corresponding peaks observed in the DTA trace, it can be deduced that this loss in mass is due to the evolution of the organic compounds present in the gel, which were added as precursors or formed due to reactions between the precursors and any alcohol that was added to the batches. The TGA trace exhibits a further loss in mass, but at a much slower rate begining at about 450 °C, up to about 800 °C. In this temperature range, mass loss occurs at a much faster rate between about 690 and 800 °C. This temperature regime in the DTA plot encompasses a region displaying a very pronounced exothermic peak at about 870 °C, with the onset of this peak at approximately 775 °C. The occurrence of the exothermic peak and the simultaneous rapid loss in mass is indicative of a probable decomposition reaction accompanied by the evolution of some of the decomposition products. Further examination of the DTA trace is further characterized by a strong endothermic peak at about 500 °C. A strong endothermic peak is characterized of the formation of some product that requires energy being supplied to the system, in order that the system may overcome any kinetic barriers and then form the product. This may indicate that the endothermic peak is associated with the formation of hydroxyapatite, if the formation of hydroxyapatite was based on a nucleation and growth mechanism. Further evidence is support of this hypotheses is obtained from the X-ray diffraction analyses and FT–IR spectral characterization of various samples of dried gel heated to different temperatures based upon indications from the DTA and TGA traces. As all four sample batches indicated similar DTA and TGA traces, representative results from one sample are presented here. A detailed study following the evolution of different phases during the heat treatment of the dried gel to form hydroxyapatite is discussed in other publications.

3.3. Formation of hydroxyapatite and characterization using X-ray diffraction and FT–IR spectroscopy

In order to characterize the reactions indicated by differential thermal analysis and to determine the formation temperature of hydroxyapatite, samples of the dried gel with an initial Ca/P ratio of 1.67 and containing ethanol, were heated at 460, 550, 775 and 1000 °C. The samples heated to 460, 550 and 775 °C were soaked at temperature for 4 h, while the sample heat treated at 1000 °C was held at temperature for 10 h. After heat treatment, the samples were air-quenched to room temperature, and the formed phases were examined using X-ray diffraction and mid-IR FT–IR spectral characterization techniques Fig. 4 illustrates the X-ray diffraction patterns obtained by heat treating the gel at various temperatures. Fig. 5 illustrates the corresponding mid-IR FT–IR spectra of the samples.

On examining Fig. 4, we observe that the pattern representative of the sample heat treated at 460 °C is

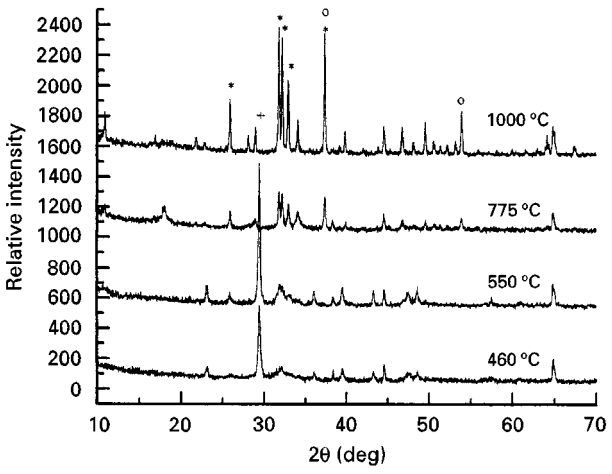

Figure 4 XRD patterns for a sample batch with 5 ml ethanol upon heat treatment at different temperatures. (*) Hydroxyapatite, (○) CaO, (+) $CaCO_3$.

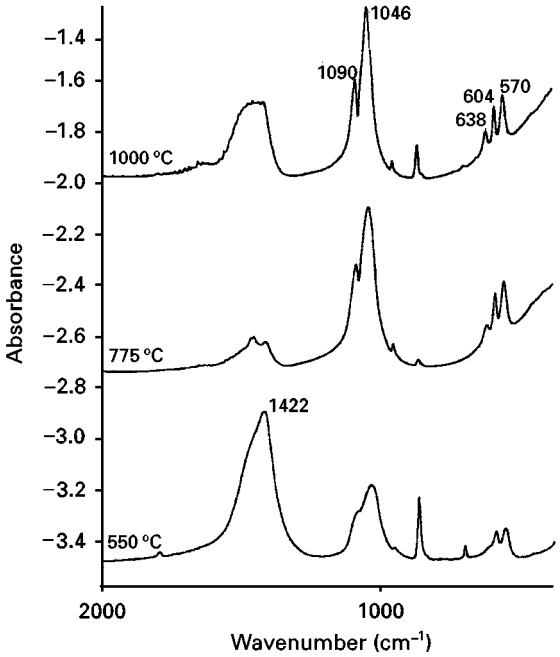

Figure 5 FT–IR spectra for sample batch with 5 ml ethanol upon heat treatment at different temperatures.

characterized by a very strong peak at 29.4° 2θ (reflection of the (1 0 4) planes). This peak together, with a peak at 39.93° 2θ are characteristic of calcium carbonate (calcite). At this temperature, there is no evidence of any hydroxyapatite being present in the sample. The presence of hydroxyapatite would be marked by a strong X-ray peak at 31.733° 2θ, corresponding to the strongest intensity reflection of the (2 1 1) planes, and two peaks at 32.196° and 32.902° 2θ, both having equal intensities (60% relative intensity corresponding to (1 1 2) ad (3 0 0), respectively). Upon heating to 550 °C (a temperature past the endothermic peak seen in the DTA plot), the first evidence of hydroxyapatite formation is seen, by the presence of the peaks just described above. The peaks arising from reflection due to $CaCO_3$ appear unchanged. However, upon heating to 775 °C, the presence of a new peak at 37.347° 2θ angle is detected. Also, the peaks due to hydroxyapatite grow further in intensity, due to stronger reflections from the increasing quantity of hydroxyapatite in the system. The new peak at 37.347° together with the peak at 53.856° 2θ correspond to reflections from calcium oxide, CaO. Interestingly, this temperature region corresponds to a region of rapid mass loss in the TGA plot. At this temperature, there is still plenty of $CaCO_3$ present in the system. Heating to 1000 °C, however, eliminates the peaks due to $CaCO_3$. Also, at this temperature, the peaks due to hydroxyapatite are very well defined, and the system indicates the presence of a significant quantity of CaO. Thus, it is observed that the formation of hydroxyapatite is initiated at a relatively low temperature and can be associated with the endothermic reaction observed at about 500 °C. In order to increase the quantity of hydroxyapatite in the system, the batch has to be heated to a higher temperature, and at a temperature about 900 °C, decomposition of $CaCO_3$ occurs by the formation of CaO and evolution of CO_2. It may be safely assumed that formation of $CaCO_3$ is due to reactions between the carbonates being evolved at low temperatures upon heating to drive out the organics in the gel, and the extremely reactive calcium present in the gel.

An examination of the FT–IR spectral data indicates a very similar trend in the spectral characteristics. The FT–IR spectra of the sample at 550 °C is characterized by a very intense band at 1422 cm^{-1}. This band can be attributed primarily due to the vibrations of the carbonate ions. The very broad nature of the band also indicates the possible presence of other organic species such as $-CH=CH_2$, or $-COO^-$ groups, all of which may be formed due to reactions between the evolved organics and calcium. The very first indications of the formation of hydroxyapatite are also visible, in the form of a broad IR band centred at about 1046 cm^{-1} with a very weak shoulder at about 1090 cm^{-1}. The spectrum at 775 °C shows a significant increase in the intensity of the bands at about 1046 and 1090 cm^{-1}. These bands arise due to the factor group splitting of the ν_3 fundamental vibrational mode of the PO_4^{3-} tetrahedra. This fundamental mode corresponds to the triply degenerate asymmetric P–O stretching modes. Similarly, the band at about 960 cm^{-1} is observed as a discernible band. This band corresponds to the ν_1 symmetric P–O stretching vibrations of the PO_4^{3-} ion. The distinguishable presence of these bands together with the bands at about 604 and 570 cm^{-1} corresponding to the triply degenerate ν_4 bending vibrations of the PO_4^{3-} ions indicate the increased quantity of hydroxyapatite in the batch at this temperature. Also, the bands corresponding to the doubly degenerate ν_3 vibrations of calcite in the region 1429–1492 cm^{-1} show a drastic decrease in intensity. The spectrum of the sample heat treated at 1000 °C shows the bands corresponding to hydroxyapatite to be well pronounced. The presence of CaO cannot be detected as bands corresponding to the Ca–O stretching modes would lie in the near IR region at wave numbers below 400 cm^{-1}, which is below the detection threshold of the instrument used.

Thus, heat treatment at 1000 °C does produce hydroxyapatite along with calcium oxide. In order to eliminate the calcium oxide present in the sample, the reactivity of calcium oxide can be used to our advantage. Upon treatment of the sample batch with 0.01 M HCl acid solution, the calcium oxide gets converted to calcium chloride. Hydroxyapatite exhibits far less reactivity to the HCl solution than the calcium oxide. Further, due to the high solubility of calcium chloride in water, as compared to the limited solubility of hydroxyapatite in water, the calcium chloride is eliminated from the system. Conversion of calcium oxide to calcium chloride and then the latter's elimination was achieved by adding the sample powder heat treated at 1000 °C to the 0.01 M HCl solution, followed by rapid stirring for 2 h, filtering and washing the residue with distilled water along with drying the residue at 120 °C for 2 h. Fig. 6 indicates the X-ray diffraction pattern of the sample batch heat treated at 1000 °C prior to the HCl treatment, and after HCl treatment. After washing in HCl, the powder patterns do not indicate any

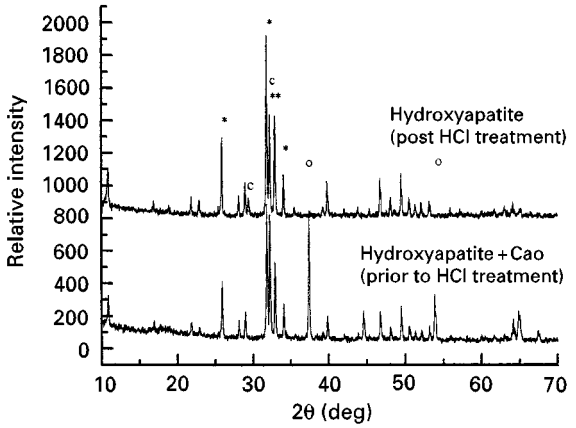

Figure 6 XRD patterns of a sample batch with 5 ml ethanol, (a) prior to and (b) post HCl treatment. (∗) Hydroxyopatite, (○) CaC, (c) carbonate hydroxyapatite.

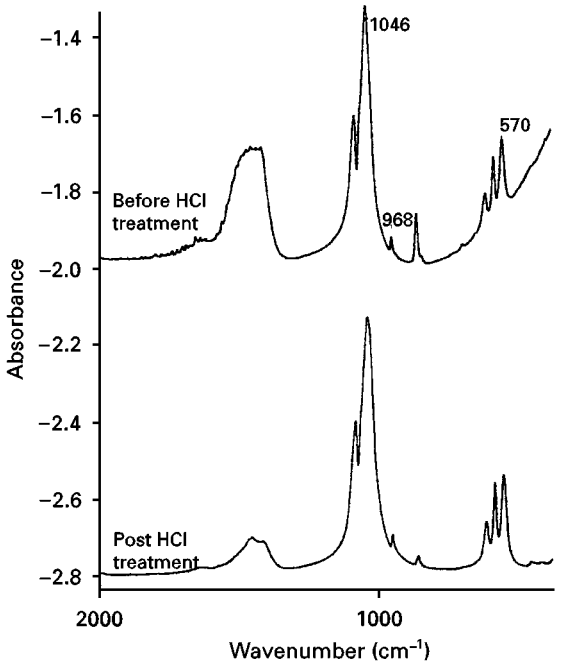

Figure 7 FT–IR spectra of a sample batch with 5 ml ethanol, (a) prior to and (b) post HCl treatment.

peaks corresponding to CaO. However, a small new peak is observed at 29.38° 2θ. This peak was not observed in any of the XRD patterns before the HCl treatment. Together with the FT–IR spectra illustrated in Fig. 7, indicating the spectra of the sample batch heat treated at 1000 °C, prior and post treatment with HCl, this peak may be assigned to correspond to carbonate hydroxylapatite. The assignment of this peak as belonging to carbonate hydroxylapatite can be done with some confidence, based on the FT–IR spectra illustrated in Fig. 8, indicating a low intensity broad band in the region ∼1410–1840 cm^{-1}. Fig. 8 shows a comparison of the FT–IR spectra of the four sample batches heat treated at 1000 °C, after HCl treatment. A detailed examination of the aforementioned band indicates a fine structure to this broad band comprising some barely discernible peaks at ∼1416 and 1460 cm^{-1}. Moens *et al.* [22] have ascribed the bands at 872, 1417 and 1460 cm^{-1}

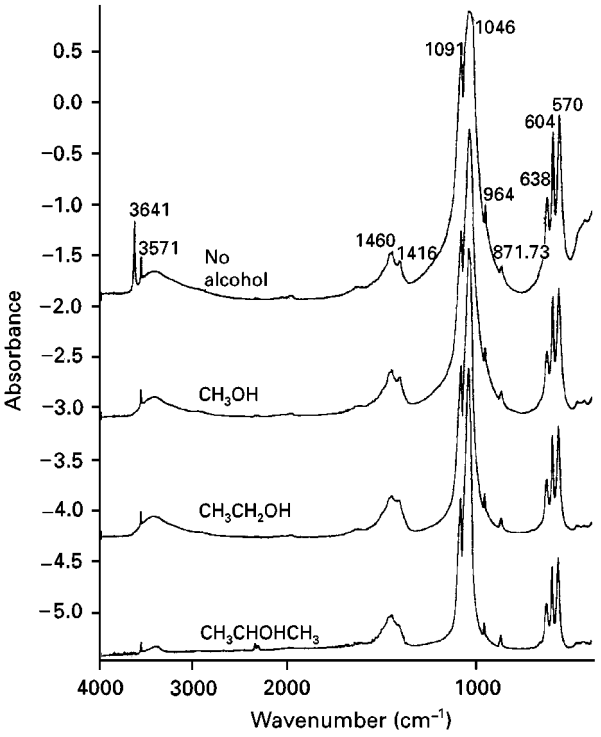

Figure 8 FT–IR spectra of sample batches with varying R–OH post HCl treatment.

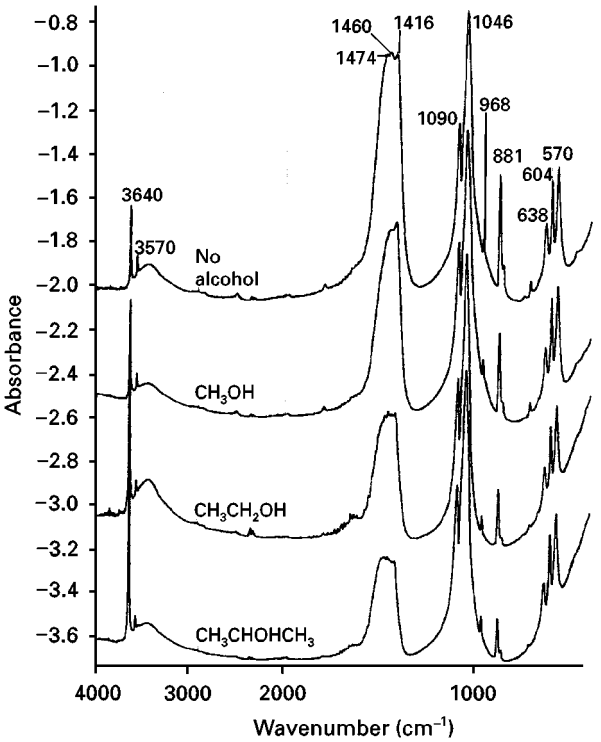

Figure 9 FT–IR spectra of sample batches with varying R–OH prior to HCl treatment.

to belong to the B-type carbonate hydroxyl apatite, in which some of the CO_3^{2-} ions substitute for the PO_4^{3-} ions. The same bands are also observed in Fig. 9, which shows the FT–IR spectra of the four sample batches upon heat treatment at 1000 °C, prior to HCl treatment. Clear identification of this variant using XRD is clouded by the fact that the strongest

reflections of this compound arising from the (1 1 2) planes lie at 32.199° 2θ, which almost overlaps the 60% relative intensity reflection of hydroxyapatite arising from the (1 1 2) planes, that lie at 32.196° 2θ. The lack of peaks corresponding to the carbonate hydroxyl apatite in the X-ray diffraction patterns of the sample batches heat treated at 1000 °C, prior to HCl treatment, may be due to incomplete crystallization of this phase, which may crystallize further upon reaction in an aqueous environment. The crystallization of the carbonate hydroxyl apatite may be aided by the presence of any amorphous calcium phosphate that may be present in the sol–gel batch [23].

Fig. 10 illustrates the Raman spectra of the four sample batches heat treated at 1000 °C, after HCl treatment. As can be seen from Figs. 8 and 10, there are no discernible differences in the spectra of hydroxyapatite produced from the four batches containing various carbon chain alcohols, and no alcohol in the last case. The Raman spectrum for hydroxyapatite obtained from the sample batch with 5 ml ethanol illustrated in Fig. 11 illustrates four distinguishable groups of spectral bands. The first group consists of two bands at ~432 and 442 cm^{-1}. These bands correspond to the factor group splitting of the ν_2 bending vibrations of the PO_4^{3-} ion. The bands present at ~579, 592 and 608 cm^{-1} belong to the ν_4 fundamental vibrational mode and arise from the triply degenerate bending vibrations. The very intense band at 962 cm^{-1} arises from the symmetric stretching modes and is designated as the ν_1 fundamental vibrational mode. The bands comprising the fourth group arise from the ν_3 fundamental vibrational modes and are due to the asymmetric stretching vibrations of the P–O bonds. These bands are seen at ~1025, 1047, 1075 and 1087 cm^{-1}.

Fig. 12 compares the XRD patterns of the four sample batches prior to the HCl treatment. No discernible differences are observed between the four sample batches, all of them indicating the presence of hydroxyapatite and calcium oxide. Comparing this figure with Fig. 13 which displays the X-ray diffraction patterns of the four sample batches after HCl

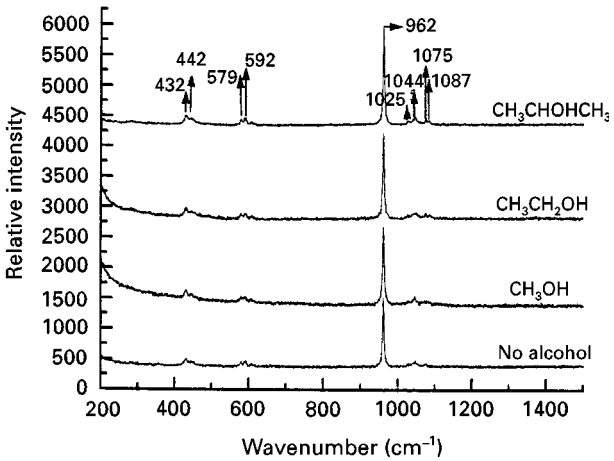

Figure 10 Raman spectra of sample batches with varying R–OH post HCl treatment.

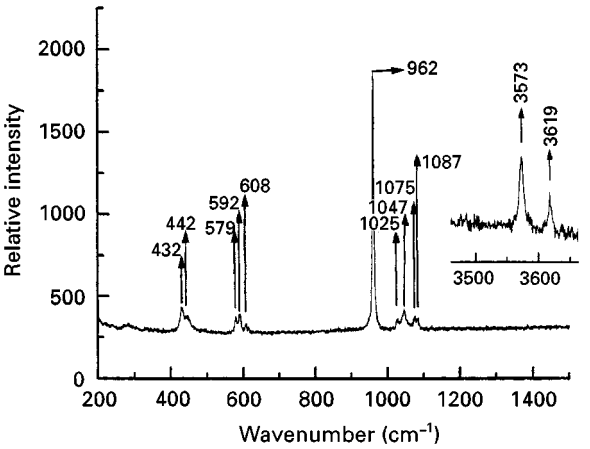

Figure 11 Raman spectrum of hydroxyapatite (synthesized from a batch containing 5 ml ethanol).

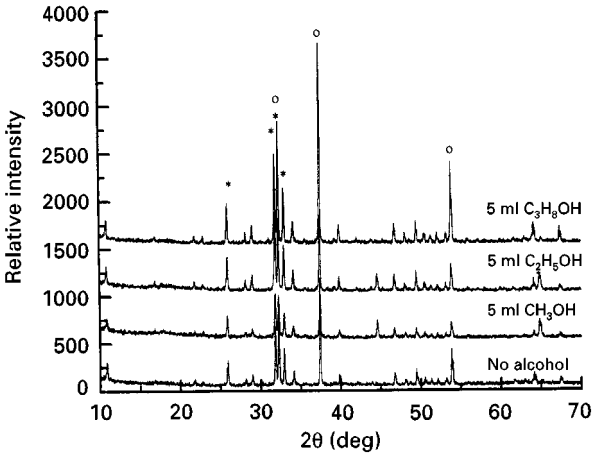

Figure 12 XRD patterns of sample batches with varying R–OH prior to HCl treatment. (○) CaO, (*) hydroxyapatite.

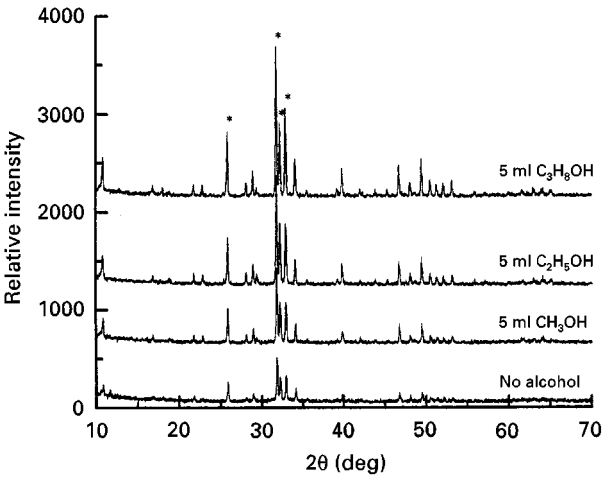

Figure 13 XRD patterns of sample batches with varying R–OH post HCl treatment. (*) Hydroxyapatite.

treatment, one observes that calcium oxide is eliminated from all of the samples. However, the peak at 29.38° 2θ which was ascribed to the formation of carbonate hydroxyapatite is present in all four patterns. The presence of carbonate hydroxyapatite is

TABLE I ICP results for Ca/P ratios in hydroxyapatite synthesized from the four sample batches. Ca/P weight ratios reported are averages of three measured values for each batch

Sample batch	Ca/P weight ratio	Standard deviation
Ideal stoichiometric HA	2.157	
Batch with no alcohol	2.295	0.014
Batch containing methanol	2.167	0.015
Batch containing ethanol	2.282	0.009
Batch containing propanol	2.497	0.014

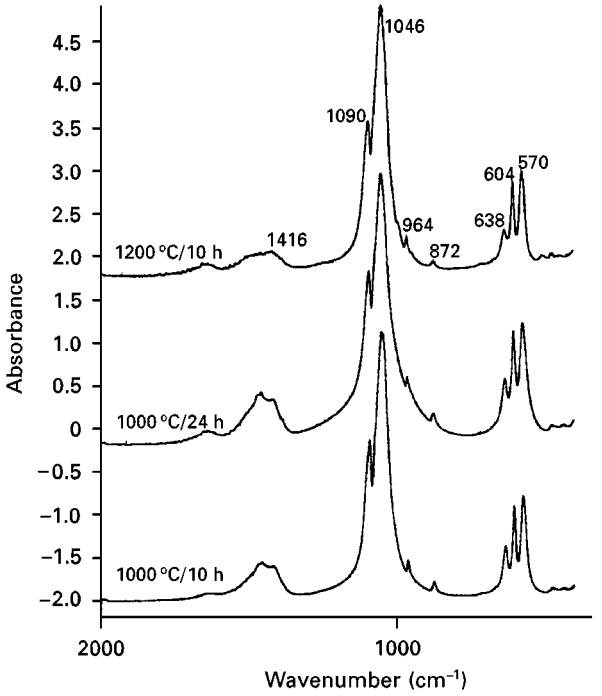

Figure 14 FT–IR spectra of a sample batch with 5 ml ethanol upon heat treatment (a) 1000 °C/10 h, (b) 1000 °C/24 h, and (c) 1200 °C/10 h.

also confirmed from the ICP analysis result of synthesized hydroxyapatite batches. These results are summarized in Table I. Stoichiometric hydroxyapatite had a Ca/P weight ratio of 2.157. Any substitution of phosphate ions by carbonate ions will lead to an increase in the Ca/P ratio of the sample. As is observed, the Ca/P weight ratio of the samples is found to vary from 2.167–2.497 for the sol–gel batch with propanol addition. It can be deduced that formation of the carbonate apatite occurs during the HCl treatment. The incorporation of carbonate into the hydroxyapatite lattice is due to residual carbonates from the incomplete elimination of the carbonates during the organic burn-out stage.

Holding the samples at 1000 °C for extended periods of time did not produce any discernible changes. Fig. 14 illustrates the FT–IR spectra for the sample batch containing 5 ml ethanol, upon heat treatment at (a) 1000 °C for 10 h (b) 1000 °C for 24 h. As is observed, there are no difference in the spectra. However, increasing the treatment temperature to 1200 °C and holding for 10 h appears to reduce the amount of carbonate hydroxyl apatite. This may be explained by

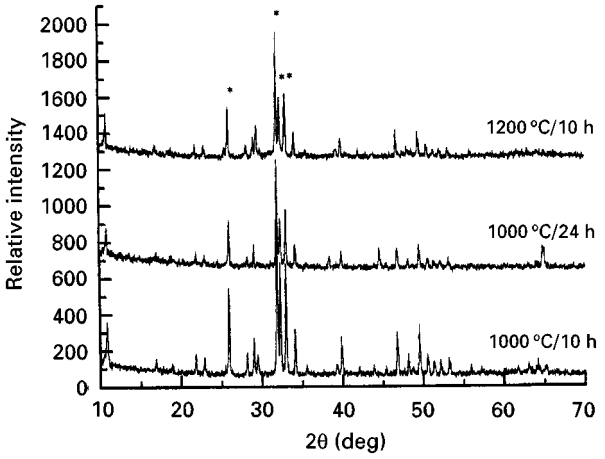

Figure 15 XRD patterns of sample batch with 5 ml ethanol upon heat treatment (a) 1000 °C/10 h, (b) 1000 °C/24 h, and (c) 1200 °C/10 h. (*) Hydroxyapatite.

the fact that the higher heat-treatment temperatures eliminate any residual carbonates to a greater extent, thereby leaving far smaller quantities that can crystallize as carbonate hydroxyl apatite upon HCl treatment. This same trend is also viewed in the X-ray diffraction patterns illustrated in Fig. 15.

4. Conclusion

Hydroxyapatite was synthesized using the sol–gel route with calcium acetate and triethyl phosphate as precursors. The gel formed was a colloidal gel, and hence, difficulties associated with the slow rates of hydrolysis of phosphates were overcome. Different batches made with additions of methanol, ethanol, propanol or no alcohol at all, indicated no significant differences in the final product formed. Owing to the incomplete removal of organics during heat treatment, it appears that batches made without the addition of any alcohol would be the most ideal way to sol–gel process hydroxyapatite with this precursor system. Formation of hydroxyapatite occurs at a relatively low temperature of about 500 °C. However, in order to increase the yield of hydroxyapatite, and to eliminate the carbonates present in the system, heat treatment to a higher temperature is essential. The formation of calcium oxide, due to decomposition of calcium carbonate occurs in the temperature range of about 780–900 °C. This calcium oxide can be eliminated by conversion to calcium chloride by stirring the powder in a HCl solution, and then dissolving the calcium chloride in water, while leaving behind the hydroxyapatite phase.

References

1. R. Z. LEGEROS and J. P. LEGEROS, in "An Introduction to Bioceramics", edited by L. L. Hench and J. Wilson (World Scientific, Singapore 1995) p. 139.
2. E. C. SHORS and R. E. HOMES, *ibid*., p. 181.
3. F. J. CALLENS, R. M. H. VERBEECK, D. NAESSENS, P. F. A. MATTHYS and E. R. BOESMAN, *Calc. Tissue Int.* **44** (1989) 114.

4. F. J. CALLENS, R. M. H. VERBEECK, P. F. A. MATTHYS, L. C. MARTENS, E. R. BOESMAN and F. C. M. DRIESSENS, *Bull. Soc. Chim. Belg.* **96** (1987) 165.
5. W. E. BROWN and L. CHOW, *Ann. Res. Mater. Sci.* **6** (1976) 213.
6. S. R. LEVITT, P. H. CRAYTON, E. A. MONROE and R. A. CONDRATE St, *J. Biomed. Mater. Res.* **3** (1969) 683.
7. H. AOKI and K. KATO, *Ceram. Jpn* **10** (1975) 469.
8. T. HATTORI, Y. IWADATE and T. KATO, *Adv. Ceram. Mater.* **3** (1988) 426.
9. A. C. TAS, F. KORKUSUZ, M. TIMUCIN and N.AKKAS, *J. Mater. Sci. Mater. Med.* **8** (1997) 91.
10. R. N. CORREIA, M. C. F. MAGALHAES, P. A. A. P. MARQUES and A. M. R. SENOS, *J. Mater. Sci. Mater. Med.* **7** (1996) 501.
11. E. LERNER, S. SARIG and R. AZOURY, *ibid.* **2** (1991) 138.
12. P. W. BROWN and M. FULMER, *J. Am. Ceram. Soc.* **74** (1991) 934.
13. P. W. BROWN, N. HOCKER and S. HOYLE, *ibid*, **74** (1991) 1848.
14. T. KAMIYA and H. MONMA, *J. Mater. Sci.* **22** (1987) 4247.
15. T. HATTORI, Y. IWADATE, H. INAI, K. SATO and Y. IMAI, *Yogyo-Kyokai-Shi.* **95** (1987) 825.
16. K. KAMIYA, T. YOKO, K. TANAKA and Y. FUJIYAMA, *J. Mater. Sci.* **24** (1987) 827.
17. J. HU, D. K. AGARWAL, Y. FANG and R. ROY, *ibid.* **28** (1993) 5297.
18. J. LIVAGE, P. BARBOUX, M. T. VANDERBORRE, C. SCHMUTZ and F. TAULELLE, *J. Non-Cryst. Solids* **147/148** (1992) 18.
19. A. DEPTULA, W. LADA, T. OLCZAK, A. BORELLO, C. ALVANI and A. Di BARTOLOMEO, *ibid.* **147/148** (1992) 537.
20. C. CHAI, B. BEN-NISSAN, S. PYKE and L. EVANS, *Mater. Manuf. Processes* **10** (1995) 205.
21. R. A. McIVOR, D. G. McCARTY and G. A. GRANT, *Can. J. Chem.* **34** (1956) 1819.
22. P. MOENS, F. CALLENS, P. MATTHYS, F. MAES, R. VERBEECK and D. NAESSENS, *J. Chem. Soc. Farad. Trans.* **87** (1991) 3137.
23. L. L. HENCH and O. ANDERSON, in "An Introduction to Bioceramics", edited by L. L. Hench and J. Wilson (World Scientific, Singapore 1993) p. 41.

Received 21 September 1997
and accepted 15 May 1998